Postprint of: Zoupas L., Wodtke M., Papadopoulos C.I., Wasilczuk M., Effect of manufacturing errors of the pad sliding surface on the performance of the hydrodynamic thrust bearing, Tribology International, Vol. 134 (2019), pp. 211-220, DOI: 10.1016/j.triboint.2019.01.046.

Effect of manufacturing errors of the pad sliding surface on the performance of the hydrodynamic thrust bearing

Loukas Zoupas[1], Michał Wodtke[2], Christos I. Papadopoulos[1], Michał Wasilczuk[2]

[1] *School of Naval Architecture and Marine Engineering, National Technical University of Athens, Zografos, Greece*

[2] *Gdansk University of Technology, Faculty of Mechanical Engineering, Gdansk, Poland*

Abstract

In the present study, investigation of the effect of manufacturing errors on the performance of large tilting pad thrust bearings has been performed, following a CFD-based Thermohydrodynamic analysis of a single pad. A 3D model has been generated, including the pad, the lubricant film and the corresponding part of the collar. The pad has been assumed to be deformed about the pivot point, due to thrust loading. Manufacturing errors of different type and amplitude have been superimposed. The equilibrium position of the pad has been calculated by a Newton-Raphson iterative procedure. The principal performance parameters of the bearing (minimum film thickness, friction torque, maximum pressure and temperature) have been calculated. The results demonstrate that manufacturing errors may affect substantially bearing performance, and should be taken into consideration in the design of large tilting pad thrust bearings.

Keywords: THD, Tilting-pad Thrust Bearing, CFD, Manufacturing Errors.

1. Introduction

In normal operating conditions, properly designed fluid film bearings operate in the regime of full film lubrication, with rubbing surfaces being completely separated by a lubricating film. Depending on bearing type, operating conditions and lubricant type, the thickness of the lubricating film may range between a few micrometers and several tens of micrometers. In computational analyses of such bearings, a common assumption is to consider the sliding surfaces as geometrically ideal. In practice, such an assumption is not realistic because of manufacturing imperfections, which always occur despite the precise contemporary manufacturing techniques. Manufacturing inaccuracies can be more pronounced in bearings of large size, in which the area of machining is large. Usual machining tolerances are within the range of 20 micrometers, which in many cases is comparable to the value of minimum film thickness during bearing operation.

Apart from machining inaccuracies, the shape of sliding surface during operation is also a result of bearing loads, which cause deformations due to temperature distribution and film pressure. In many cases, these effects are nowadays taken into account in theoretical analyses, while the effect of manufacturing imperfections – including roughness, waviness, non-planarity and also wear of the sliding surfaces has

been very rarely investigated before. In these few studies, the performance of journal bearings with defects in geometry has usually been investigated. For example, in their works Burton [1] and Li with Chen [2] theoretically investigated the influence of surface roughness on bearing properties. Changes in gas bearings' characteristics caused by imperfections of bearing geometry, such as ovality, conical shape and errors in circularity were theoretically studied by Pande and Somasundaram [3] and experimentally by Wilson [4]. Because of rigorous requirements for aerostatic bearings used in ultra-precision machines e.g. measuring instruments or machining tools, several recently published researches were also devoted to investigate effect of sliding surface shape errors on their performance. Wang et al. studied static [5] and dynamic performance [6] of aerostatic journal bearing including waviness of the surface in axial and circumferential direction. Cui et al. investigated effect of manufacturing errors of different shape (e.g. waviness or taper) on angular stiffness of aerostatic bearing [7] an also on static characteristics [8] and running accuracy [9] of aerostatic bearing with porous restrictor. Results of those researches revealed, that aerostatic bearing surface shape deviations influences markedly static and dynamic bearing properties.

Shelly and Ettles [10], in their calculations, determined the influence of transverse and longitudinal surface waviness, with the amplitude of 2.5 μm and circumferential length of 100 μm on steady state hydrodynamic journal bearing performance. In [11] and [12] the influence of geometrical imperfections and roughness on load carrying capacity of a radial bearing were investigated. Effect of the sliding surface roughness on transient journal bearing behavior during startup was also theoretically investigated by Cui et al. [13]. They applied mixed lubrication model considering both asperity contact and hydrodynamic effect. One of the findings of the mentioned work is, that surface roughness included in the modeling has an influence on the calculated bearing properties during initial period of bearing startup, e.g. lift-off speed or contact time. Fillon and Bouyer [14], and Litwin [15] studied the influence of local wear of the bush on bearing characteristics, while Dobrica and Fillon [16] theoretically determined the effect of circumferential scratches on bearing operation. From the studies referenced above it can generally be concluded that local imperfections of bearing shape may have noticeable influence on bearing performance. Load carrying capacity can be substantially reduced, bearing losses may be significantly altered, whereas the distributions of film pressure and temperature may also be affected. This influence is more pronounced in highly loaded bearings, in which minimum film thickness is small, becoming comparable to the size of the surface imperfections.

In the case of hydrodynamic thrust bearings, various modifications of the sliding surface shape were studied. Charitopoulos et al. [17] studied the performance of textured thrust bearings with manufacturing errors such as concavity, convexity, and waviness, demonstrating a substantial effect on the principal performance indices, either negative, but also positive in several cases, with increasing defect amplitudes. Papadopoulos et al. [18] analysed, with the use of CFD, the effect of microdimples machined on the bearing surface. Fouflias et al. [19] carried out a study of the influence of inlet chamfer and a pocket made in a fixed geometry thrust bearing on its

performance. In [20] and [21] the analysis of the influence of the hydrostatic pocket machined in a tilting pad thrust bearing was carried out. The effect of roughness on a planar thrust sliding bearing properties with the use of model basing on the solution of Reynolds equation and Newton's Second Law of Motion was investigated by Li and An [22]. The results of transient bearing properties revealed for example, that together with the increase of the mating surfaces roughness (expressed as R_a parameter) the calculated average film thickness and axial acceleration of the system also increased.

Despite all these examples, thorough and systematic analysis of the influence of manufacturing imperfections on performance of tilting pad thrust bearings has not been published before. The fact that such imperfections can considerably change bearing operation was experimentally shown by Roylance [23] and theoretically by Charitopoulos et al. [24]. Roylance compared thrust washers with an introduced convexity of 1.9 μm to the flat ones. The measured differences in minimum film thickness were up to 5 - 10 μm, which shows a considerable influence of the sliding surface profile on bearing performance. In the paper [24] it was confirmed by a series of numerical calculations, that sliding surface shape imperfections of the simple slider bearing with nominally parallel surfaces can help to build up load carrying capacity.

2. Goals of the present research

The aim of the present study is to investigate the influence of manufacturing errors on the performance of tilting pad thrust bearings. A titling-pad hydrogenator bearing is used as a reference. Details of bearing geometric and performance characteristics are presented in Section 4.

To calculate bearing performance, a 3D geometric model of a single pad of the bearing is generated, considering also the lubricating oil and the respective part of the collar. The pad is appropriately modeled to include a thin layer of Babbitt material in the surface being in contact with the lubricant. The bearing collar is assumed rigid, whereas the pad is assumed to be deformed due to application of the thrust load. The studied manufacturing errors are (a) concavity, (b) convexity, and (c) waviness with one, three or five sinewaves on the pad surface.

3. Problem Setup

Fig. 1 illustrates the method of obtaining circumferential and radial profiles of the pad sliding surface used in analysis. Pad sliding surface deformation caused by axial bearing load is simulated as a 3D parabola across two directions, namely radially and circumferentially, with its center being the pivot point of the pad. Two different bearing loads are considered. Appropriate deformation amplitudes $\mathbf{A_p}$, corresponding to different thrust loads of the bearing, are obtained from the numerical (TEHD analysis) and experimental results presented in [25]. According to TEHD results, for normal bearing load pad sliding surface shape (as a result of thermal and mechanical loads) is approximated with the use of parabola with amplitude $A_p = 20$ μm whereas for double load with amplitude $A_p = 26$ μm (case "Deformed" in Fig. 1). Manufacturing errors are superimposed on the deformed sliding surface of the bearing pad. It is assumed, that modelled manufacturing errors changes circumferential pad sliding

surface geometry, while radial pad curvature remains unchanged (see appropriate cross sections in Fig. 1). The cases of concavity and convexity are simulated with the use of a negative or positive half sinewave, respectively. Manufacturing error amplitudes $\mathbf{A_m}$ range from 0 to 20 μm.

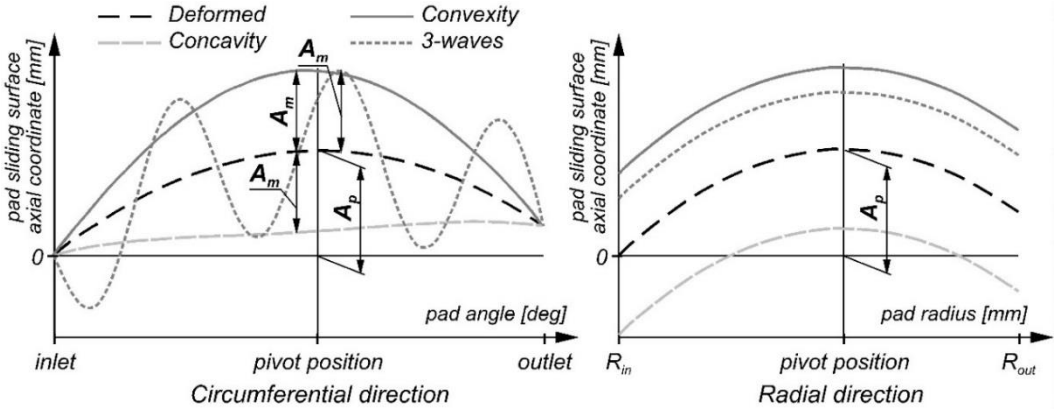

Fig. 1. Shapes of the pad sliding surface assumed for analysis (circumferential and radial cross sections at the pivot position); for the clarity of the figure only one waviness profile is shown (3-waves).

A Computational Fluid Dynamic (CFD) model is set up for calculating the tribological characteristics of the system. The model takes into consideration heat dissipation in the lubricant domain and conjugate heat transfer in the metallic parts of the bearing, thus a thermohydrodynamic (THD) solution is obtained. The conservation equations, solved with the CFD code ANSYS CFX for steady, incompressible flow, with zero gravitational and external body forces, are:

Mass conservation equation: $\nabla \cdot V = 0$ (1)

Momentum equations: $\rho(V \cdot \nabla)V = -\nabla p + \nabla \cdot (\mu \nabla V)$ (2)

Energy equation, fluid domain: $\rho c_{pf}\, V \cdot \nabla T = \nabla \cdot (\lambda_f \nabla T) - \tau : \nabla V$ (3)

Energy equation, solid domains: $\nabla \cdot (\lambda_s \nabla T) = 0$ (4)

where, V is the fluid velocity vector (m/s), p is the fluid pressure (Pa), T is the fluid/solid temperature (K), τ is the viscous stress tensor (Pa), ρ is the oil density (kg/m^3), μ is the oil dynamic viscosity (kg/(m*s)), c_{pf} is the oil specific heat capacity (J/(kg*K)), λ_f is the oil thermal conductivity (W/(m*K)), and λ_s corresponds to the thermal conductivity of the pad and the rotor (W/(m*K)).

The bearing is assumed to operate with VG46 oil; the following thermophysical properties are considered: density ρ=867 kg/m^3, heat capacity c_{pf}=2035 J/kg.K, thermal conductivity λ_f=0.13 W/m.K. Oil kinematic viscosity v is assumed temperature-dependent; its value is calculated by the McCoull-Walther's equation:

$$\text{loglog}\cdot(v+0.6) = A - B \log(T) \quad (5)$$

where A=9.382852 and B=3.67055.

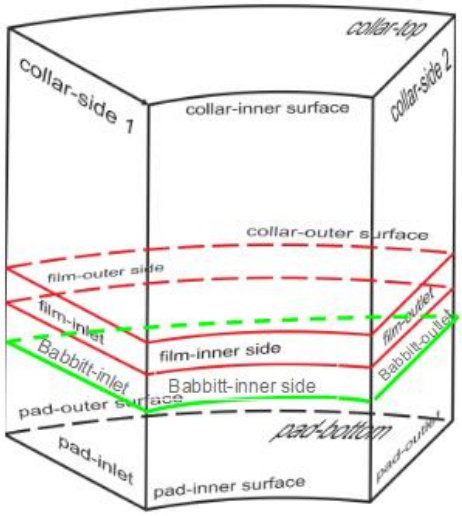

Fig. 2. Modeling of a single bearing pad: Name convention of rotor, pad, Babbitt and film boundary surfaces.

The pad and collar components are steel components; the following thermophysical properties are assumed: thermal conductivity λ_{steel}=47 W/m.K, heat capacity c_{psteel}=434 J/kg.K. The corresponding thermophysical properties of the babbitt layer of the pad are $\lambda_{babbitt}$=24 W/m.K and $c_{pbabbitt}$=230 J/kg.K.

Appropriate flow and thermal boundary conditions have been defined at each face of the computational domain, described in Fig. 2. A constant value of the convection coefficient on the free surfaces of the pad (100 W/m.K) at a reference temperature of 30^{o}C (oil supply temperature) was assumed to take into account heat transfer to the oil flowing around the pad. The adopted value is within the limits usually assumed in similar theoretical analyzes of thrust bearings [26]. In the case of the collar, on the upper and outer surfaces, where the heat transfer takes place as a result of convection to the air, a lower value of heat convection coefficient and a lower ambient temperature (25 W/m.K; 20^{o}C) was assumed. Knowledge about convection coefficients is necessary to perform analyzes, and the assumed values have an impact on the obtained results. In fact, the value of the heat convection coefficient is influenced by many factors, e.g. thermophysical properties of the fluid, the character of the velocity filed of the flow, and the shape of the heat transfer surface. However, according to the authors, changes in the shape of the oil film, as a result of presence of manufacturing errors of the sliding surface, have a small effect on flow parameters around the pad and on oil parameters, and thus have a moderate effect on the heat transfer. For this reason, the adoption of the assumptions described above allows to draw valuable conclusions from comparative analyzes made for different geometries of the sliding surface.

In order to take into account the heat transfer through the collar to other elements of the system (e.g. bearing shaft), which is characterized by lower flow resistance compared to heat convection around the pad, an increased value of heat transfer coefficient (1000 W/m.K; 30^{o}C) was assumed on the internal surface of the collar. Detailed description of boundary conditions is presented in Table 1.

Table 1. Thermal and flow boundary conditions of the model.

Collar	
Top surface / Outer surface	Heat transfer coeff: 25 W/m^2.K , T_{amb}=20^{o}C
Bottom	Fluid-Solid interface: Continuity of heat flux and temperature
Inner surface	Heat transfer coeff: 1000 W/m^2.K ,T_{amb} =30^{o}C
Sides	Periodic Conditions
Fluid Domain	
Inlet	Opening: zero relative pressure*, Opening Temp.=30^{o}C
Outer side / Outlet	Outlet: zero relative pressure*,
(*) n is the vector normal to the surface	
Babbitt	
Inlet / Inner / Outer side / Outlet	Heat transfer coeff: 100 W/m^2.K , T_{amb}=30^{o}C
Bottom	Solid-Solid interface: Continuity of heat flux and temperature
Top	Fluid-Solid interface: Continuity of heat flux and temperature
Pad	
Top	Solid-Solid interface: Continuity of heat flux and temperature
Bottom / Outer surface / Inner surface / Inlet Side / Outlet Side	Heat transfer coeff: 100 W/m^2.K , T_{amb}=30^{o}C

For a given thrust load, an iterative procedure is followed to calculate the equilibrium position of the bearing (pivot film thickness h_{pivot}, rotations about the pivot point θ_{pitch} and θ_{roll}, see details in Fig. 3). In particular, a code based on the Newton-Raphson method has been built, which takes the parameters of h_{pivot}, θ_{pitch}, θ_{roll}, and adjusts them according to the equations (6-8).

$$W - W_{req} = \oiint_S p_{HS} dxdy - W_{req} = 0 \quad (6)$$

$$M_{x,p} = \oiint_S p_{HS} x dxdy = 0 \quad (7)$$

$$M_{y,p} = \oiint_S p_{HS} y dxdy = 0 \quad (8)$$

where *S* is the bearing pad surface, W_{req} is the required thrust load, p_{HS} is the lubricant pressure after application of the Half-Sommerfeld boundary condition in the lubricant domain, calculated with the use of Eq. (9), and $M_{x,p}$ and $M_{y,p}$ are the pad moments about the x and y axis, respectively.

$$p_{HS} = \begin{cases} p \text{ if } p \geq 0 \\ 0 \text{ if } p < 0 \end{cases} \quad (9)$$

In practice, if Eq. (6) - (8) are below a given threshold (10^{-3} in this work), an equilibrium is assumed to have been reached.

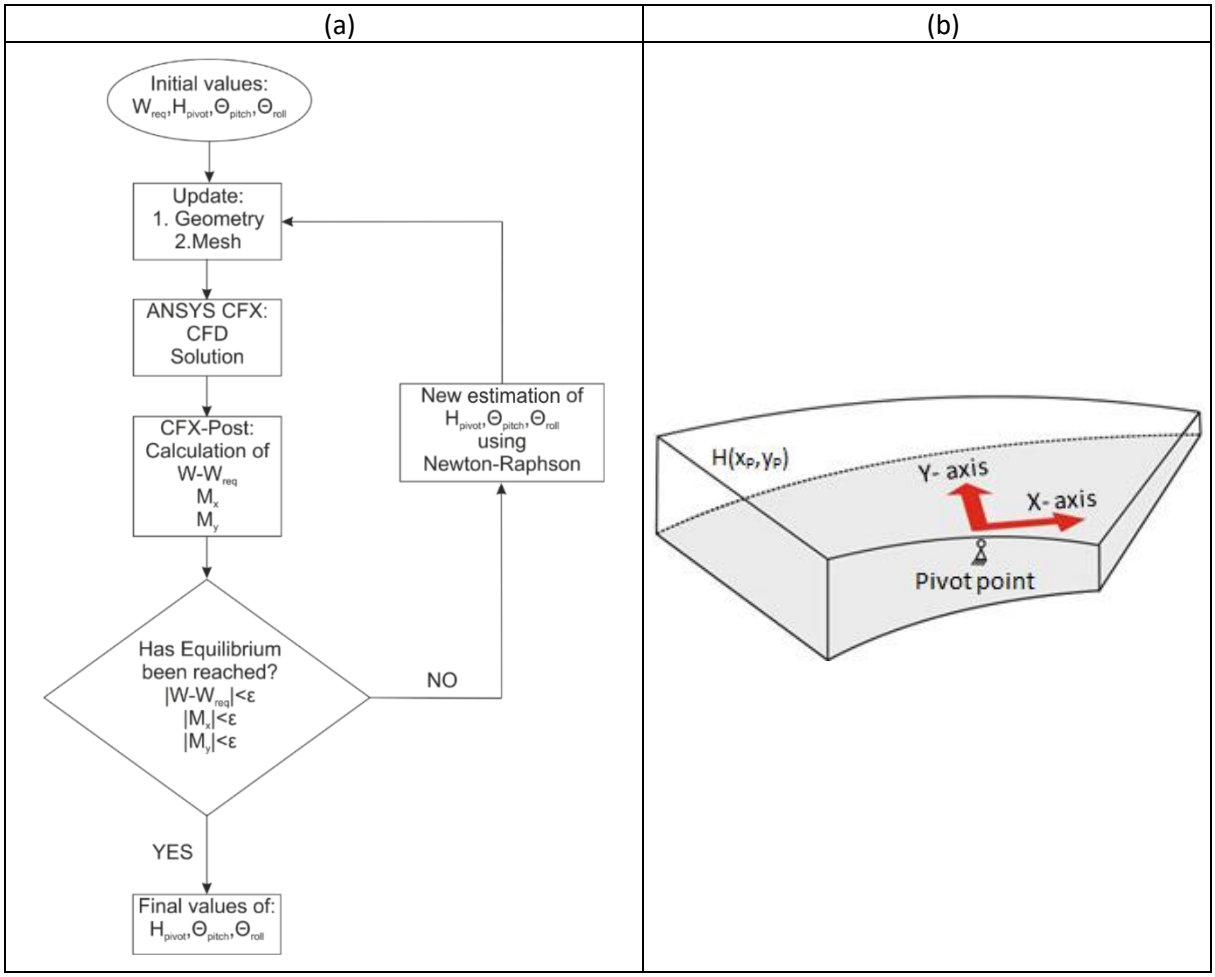

Fig. 3. (a) Iterative algorithm for obtaining equilibrium position of the bearing pad for a given thrust load. (b) Oil film geometry, pivot point and coordinate system.

Finally, the essential operating parameters of the bearing, such as minimum oil film thickness, friction torque and maximum values of pressure and temperature of the lubricant are calculated, for assessing bearing performance at a given thrust load.

4. Reference model - validation

The reference bearing used in this study was described in detail in reference [25]. It is a tilting pad bearing of a hydrogenerator. Its outer diameter is 1.8 m and other specifications are listed in Table 2. The bearing pad support is arranged in a quite common way on ring shaped disks, providing compensation of thermal crowning caused by temperature gradient and elastic deformations caused by film pressure. The bearing arrangement is shown in Fig. 4. The thrust bearing was fitted with the screw mechanism of regulating the pad height and thus theoretically providing equal sharing of load by all pads. However, the alignment seems not to be precise enough and the operation practice showed that the temperature measured in the pads differed by as much as even 18°C. The results of calculations presented in [25] indicate, that such differences of temperature can be the effect of large differences of load carried by particular pads. During operation the hottest pads could have been loaded with a double load in comparison to equal load distribution. The results of these calculations were the reason for using two load cases in the following study: a normal load of 680 kN and an overload of 1360 kN per pad.

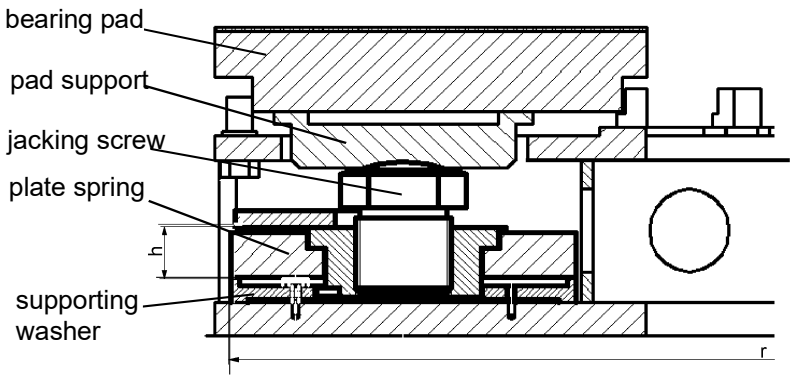

Fig. 4. Analysed thrust bearing arrangement [25]

Table 2. Thrust bearing specifications

Quantity	units	Value
number of pads	-	8
outer diameter	mm	1800
inner diameter	mm	800
pad angle	degrees	35
pivot circumferential position	degrees	18.9
pivot diameter	mm	1360
pad thickness	mm	100
collar thickness	mm	80
babbitt thickness	mm	3
supporting button diameter	mm	270
rotational speed	rpm	187.5
sliding speed (at mean bearing radius)	m/s	12.8
axial force	N	5.5×10^6
bearing specific load	MPa	2.75
lubricating oil	-	ISO VG-46
lubrication system	-	bath lubrication
high pressure jacking	-	no
oil cooling	-	coolers in the oil bath

5. Results of numerical calculations

In Fig. 5, the calculated circumferential hydrodynamic pressure profiles (at radial position corresponding to 50% of pad width - R 50%), temperature profiles (at radial position corresponding to 75% of pad width - R 75%) and film thickness profiles (at radial position corresponding to 50% of pad width) for both analyzed bearing loads are presented. The reference "*Deformed*" case corresponds to a bearing with initially perfect flat sliding surface, which is deformed thermo-elastically. The deformed pad surface shape has been calculated in a previous TEHD analysis [25]. Four additional cases with manufacturing errors are presented, namely those of concavity, convexity and waviness with one or five sinewaves. The corresponding results have been obtained with the assumption of a maximum surface shape error amplitude of 20 μm,

imposed on top of the deformed pad surface, which yields the highest impact on the operational parameters of the bearing.

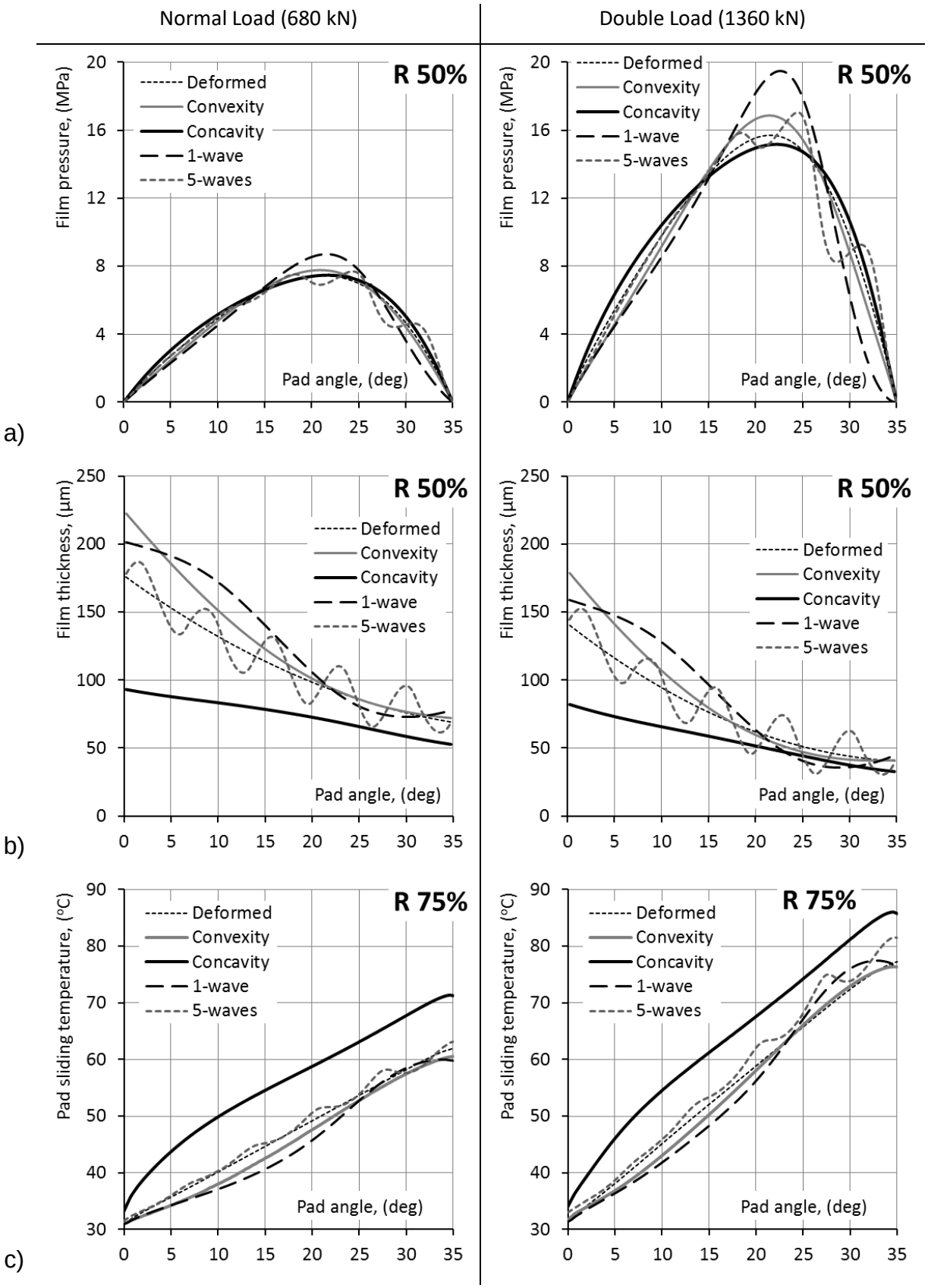

Fig. 5. Comparison of circumferential profiles for different types of manufacturing errors and bearing loads: a) film pressure at 50% of bearing width; b) film thickness at 50% of bearing width; c) pad sliding temperature at 75% of bearing width. Manufacturing error amplitude in all cases equals 20 μm.

In the left-hand column of Fig. 5, the results correspond to bearing thrust load of 680 kN (normal bearing load). The calculated circumferential pressure profiles for the cases with introduced manufacturing errors show substantial differences in comparison with the *"Deformed"* case (Fig. 5a). In particular, initial concavity of the sliding surface leads to a decrease of the film maximum pressure, while the opposite is observed for initial convexity of the pad surface. The lower maximum pressure observed in the "*Concavity*" case is compensated by increased pressure at the inflow and outflow zone, as compared to the reference case. In the case with initial convexity, the effects are reversed: higher maximum pressure is accompanied by lower inflow and outflow zone pressure. The film pressure calculated for the cases with sinewave error shapes demonstrates local pressure peaks at the ends of the local converging film segments, where film thickness attains local minima (Fig. 5b). The effect is more pronounced at areas of the pad extending from the bearing center to the outflow region. The number of pressure peaks reflects the number of the sinewaves of the modeled shape. In the case of a one-wave error shape, the maximum film pressure among all studied cases is observed.

The film profiles obtained for the five different cases also differ significantly (Fig. 5b). The introduced errors are clearly visible, as well as the differences in minimum and inlet film thickness values. Larger inlet film thickness is observed in the "*Convexity*" and "*One-wave waviness*" cases, in comparison to that of the reference "*Deformed*" case. This also implies that the circumferential inclination is larger in the former two cases. In the "*Five-wave waviness*" case, the resulting profile is oscillating about the reference case; the minimum film thickness, occurring at the top of the fourth wave, is the smallest among all studied cases except for the "*Concavity*" case. Inlet film thickness is substantially smaller in the "*Concavity*" case, in comparison to the other studied cases, so in this case the circumferential inclination of the pad is also the smallest.

Oil gap geometry influences significantly film temperature distribution, as presented in Fig. 5c, where temperature profiles are plotted at a radius located at 75% of pad width. The location was selected because it is close to the area of maximum film temperature. In general, maximum temperatures occur at the outflow region, being close to 60^{o}C for the case of normal thrust load, and close to 78 ^{o}C for the case of double thrust load. For the "*Concavity*" case, temperature is consistently 5^{o}C higher than that observed in all the other studied cases. This is due to the highest oil shear forces in the gap, given that oil film thickness in this particular case exhibits the lowest values among all analyzed cases (at the same sliding speed and load). Among the other analyzed surface shape errors, the most affected temperature profile is that corresponding to the "*Five-wave waviness*" case. In the calculated temperature profiles, local peaks of temperature values are visible in places where the film thickness attains local minima, due to locally increased oil shear stresses.

The effect of manufacturing errors on bearing performance characteristics is more pronounced as bearing thrust load increases. In the right-hand column of Fig. 5, film pressure, thickness and pad temperature distributions are presented for the case of

bearings loaded with thrust load of 1360 kN (double bearing load). Regarding film pressure, it can be observed that introduction of one-wave waviness surface error, leads to an increase of maximum pressure by 1.3 MPa, in comparison to the reference bearing under the same thrust load. On the contrary, when the bearing is operated at double load (1360 kN), the corresponding pressure increase is 3.8 MPa, which may affect substantially bearing endurance at that operational regime. Further, increased bearing thrust load leads to substantial reduction of the circumferential pad inclination, leading to reduction of minimum film thickness and increasing the maximum sliding surface temperature. The effect of manufacturing errors on the outflow oil temperature is also more pronounced when the bearing is highly loaded, for all the studied cases.

In Fig. 6 and Fig. 7, pressure and film thickness distributions at the pad surface are presented for all the studied cases; here an error amplitude of 20 μm has been considered.

Both thrust loads of the bearing are assessed. A comparison of the results indicates only small differences between the reference case and the “Concavity” and “Convexity” cases (“Convexity” case not shown in Fig. 6). More pronounced differences are observed in the case of waviness errors, where the local pressure peaks associated with the reduction in the thickness of the lubricating film in the areas of local convexity of the sliding surface profile are clearly visible. The oil pressure contours in the film are similar for the two bearing loads analyzed.

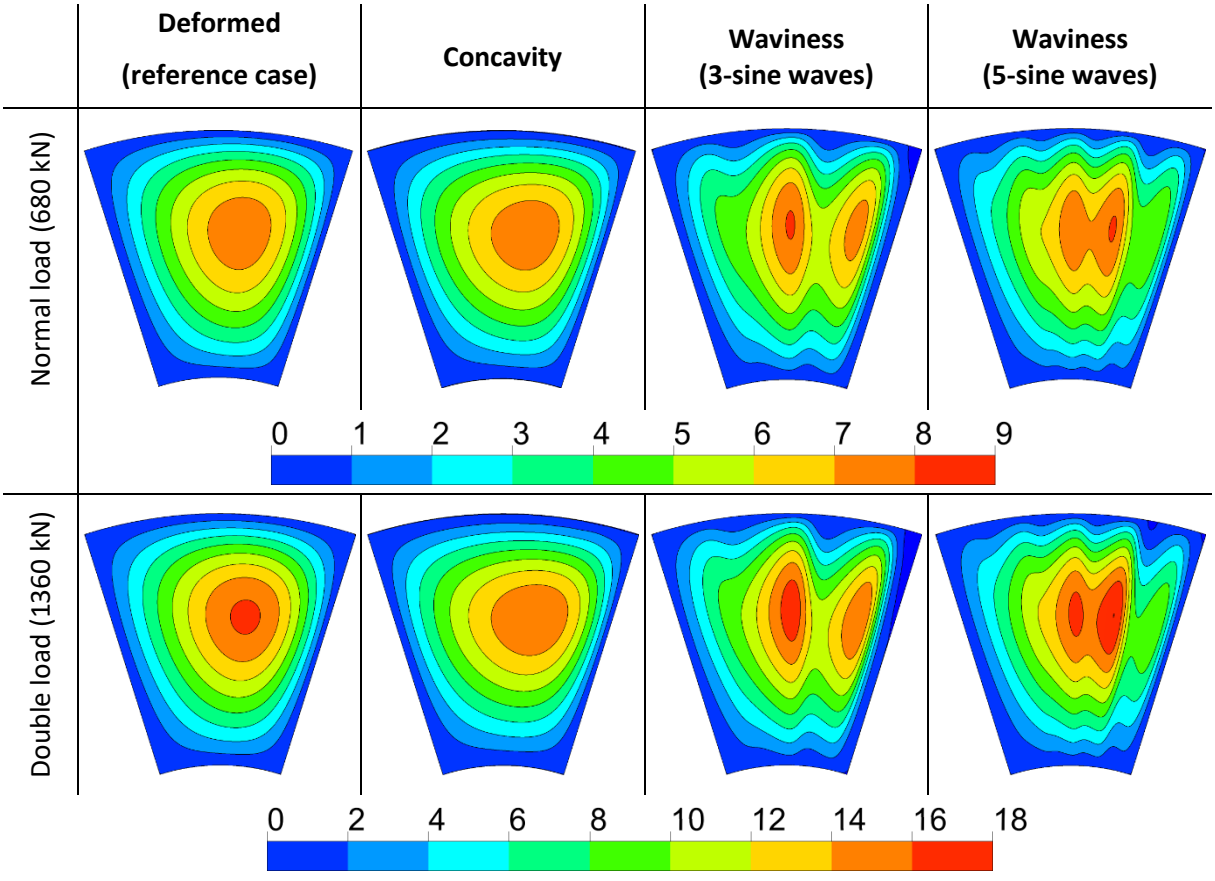

Fig. 6. Comparison of film pressure contours [MPa] for different assumed shapes of manufacturing errors with 20 μm error amplitude and both analyzed bearing loads (clockwise collar rotation).

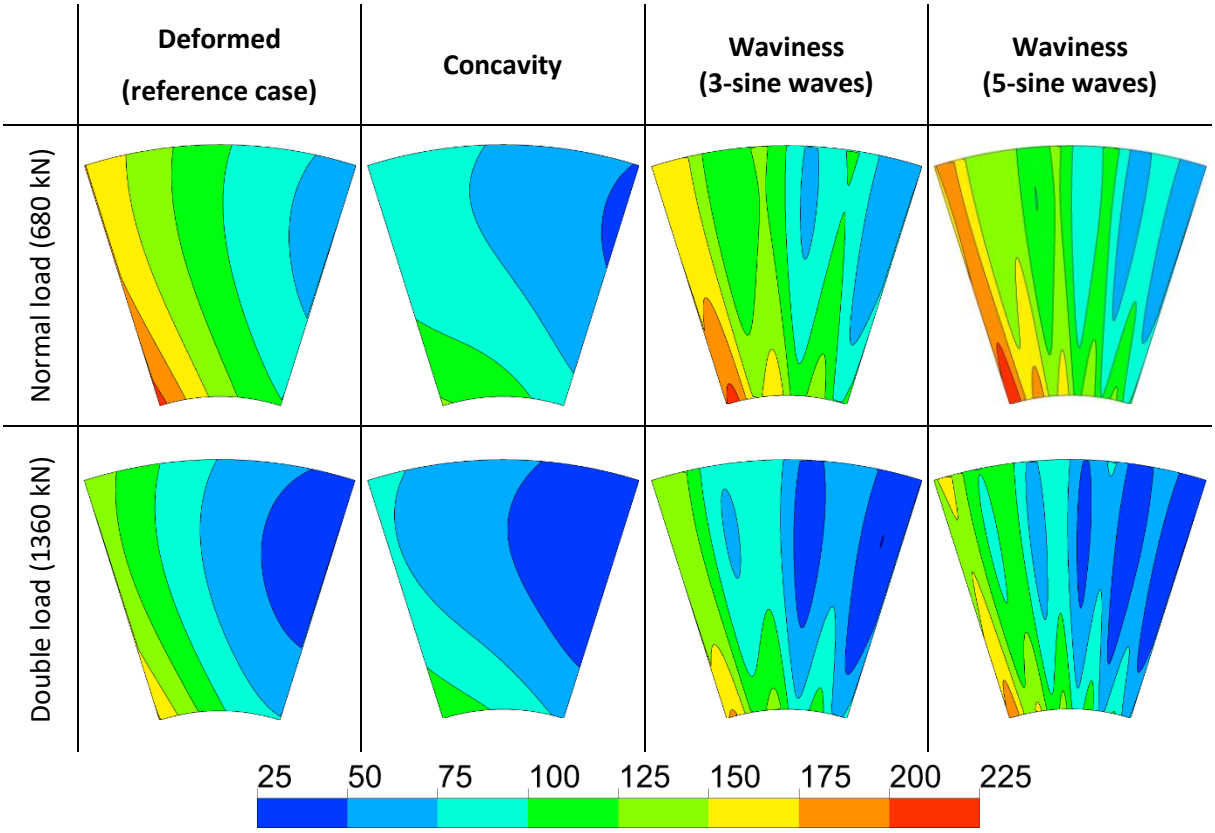

Fig. 7. Comparison of film geometry [µm] for different assumed shapes of manufacturing errors with 20 µm error amplitude and both analyzed bearing loads (clockwise collar rotation).

The geometry of the oil gap for the case of the pads with the introduced surface shape errors is noticeably different from the reference case without the shape errors (Fig. 7). The pad with a concave sliding surface exhibits much smaller film thickness values over the entire surface (lower thickness at the inlet and outlet). In this case, the minimum film thickness is located at the outflow edge of the segment. In the cases of surface waviness error, the minimum film thickness occurs at the tops of waves near the outlet area. An increase in the thrust load acting on the bearing segment results in reduction of minimum film thickness, while reducing at the same time the circumferential tilt angle of the pad.

In Fig. 8, the principal bearing performance parameters (maximum pressure, minimum film thickness, maximum temperature, friction power loss) are presented as a function of the magnitude of the manufacturing error, for different types of errors applied to the bearing pad surface. Results are presented for two thrust loads of the bearing. The magnitude of the introduced surface shape errors is shown on the horizontal axis. Values for the shape error amplitude equal to 0 µm correspond to the reference bearing case ("*Deformed*" case), characterized by an initially perfect flat sliding surface, which is deformed thermo-elastically.

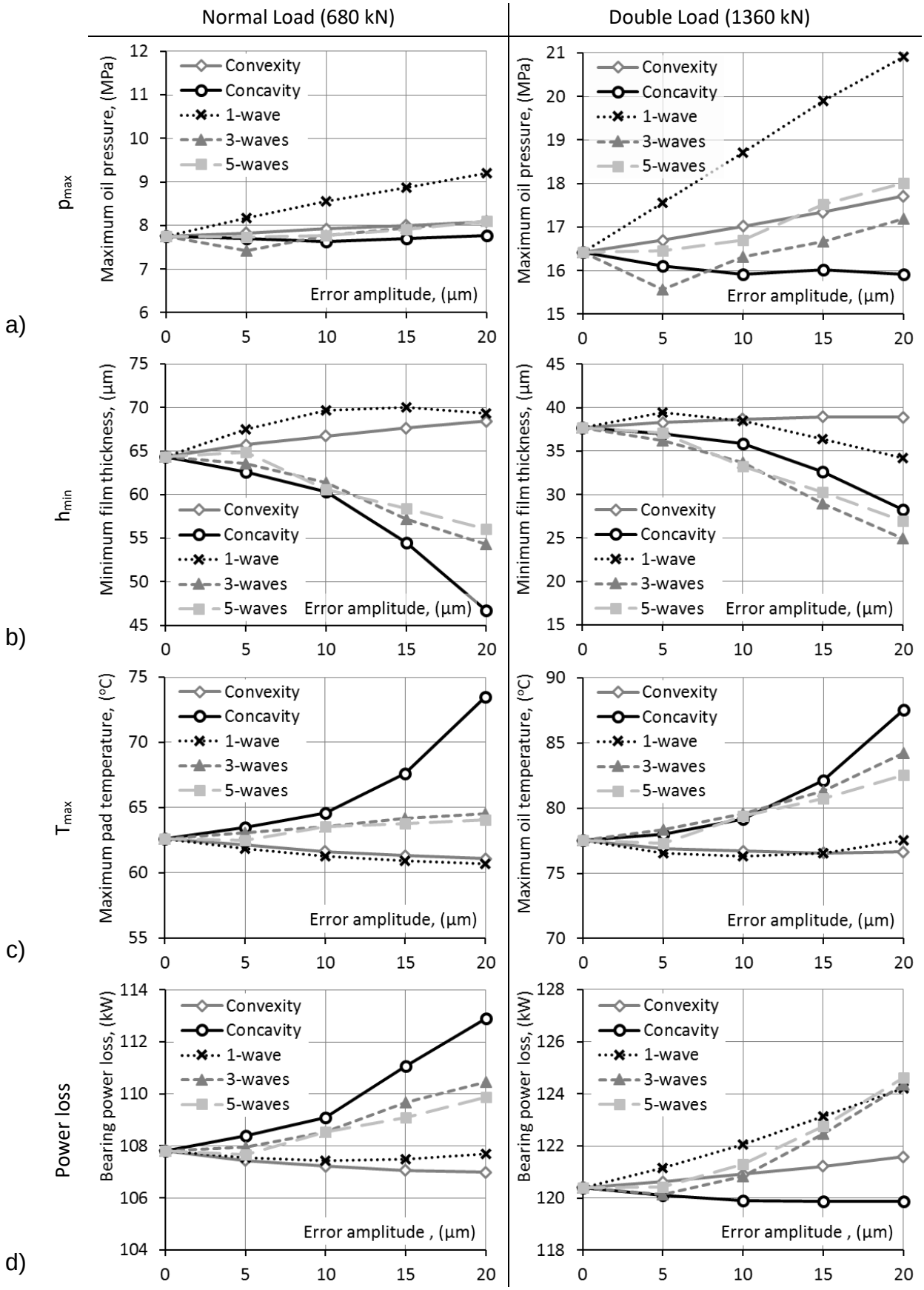

Fig. 8. Principal bearing performance parameters as a function of manufacturing error amplitude, for two different bearing thrust loads; a) maximum film pressure p_{max}; b) minimum film thickness h_{min}; c) maximum pad sliding surface temperature T_{max}; d) bearing power loss.

For the normal bearing load (680 kN), the error amplitude of the sliding surface has limited effect on the maximum film pressure (maximum approx. ± 0.4 MPa, approx. 5%, Fig. 8 a), except for the case of "*One-wave waviness*", in which a steady increase (approximately linear) of the maximum pressure value is observed, as the magnitude of the surface shape error increases. In this particular case, for the highest error value analyzed (20 μm), the maximum film pressure is higher by approx. 1.5 MPa (~ 20%) in comparison to that corresponding to the pad with no shape errors. Regarding double bearing load (1360 kN), the effect of error amplitude on bearing maximum pressure is more pronounced, but follows the same trends. In particular, for the "*One-wave waviness*" case, the highest error amplitude of 20 μm yields a difference in maximum pressure of approx. 4.5 MPa (~ 27%), in comparison to the reference bearing. In general, increase of the error amplitude increases p_{max} for pads with convexity and surface waviness errors (by maximum 1.6 MPa; ~ 9.7%) and slightly reduces p_{max} for a pad with a concave surface error (by 0.5 MPa; ~ 3%).

For the bearing normal load (680 kN), as the error magnitude increases, minimum film thickness h_{min} decreases for the cases of "Concavity", "Three-wave waviness" and "Five-wave waviness", in comparison to the reference case (Fig. 8 b). The opposite trend, i.e. increase of h_{min} with increasing error magnitude, can be observed for the "*Convexity*" and "*One-wave waviness*" cases, for error magnitudes less than 15 μm. The smallest film thickness among all analyzed cases was determined for the "*Concavity*" case, with the highest error amplitude leading to a value of h_{min} of approximately 47 μm, being 17 μm less (~ 26%) than that of the reference pad. On the other hand, the highest increase in h_{min} was 5 μm (~ 8%), observed in the "One-wave waviness" case for an error amplitude of 20 μm. When bearing operates at double load (1360 kN), the effects of error amplitude on minimum film thickness follow similar trends, but are less pronounced in magnitude.

The smallest values of film thickness were observed for the "Three-wave waviness" and "Five-wave waviness" cases (25 μm and 27 μm, respectively). The corresponding reductions of minimum film thickness, in comparison to that of the reference pad shape are 13 μm (~ 34%) and 11 μm (~ 29%), respectively. An interesting trend is observed for the case of "One-wave waviness": initially, for an error amplitude of 5 μm, h_{min} increases slightly, but then decreases, reaching a minimum of 34 μm (a decrease of ~ 10% compared to the surface without shape errors). The largest increase in film thickness for the highest magnitude of error was observed in the "Convexity" case (increase by 2 μm, ~ 5%). Based also on the results of Fig. 5 b, this behavior can be attributed to the transition of the h_{min} location from the outflow edge (as in the case of a surface without error) towards the center of the bearing.

Trends of changes in the maximum temperature of the sliding surface T_{max} for the analyzed cases are similar for both bearing loads (Fig. 8 c). The largest increase in T_{max} with respect to the reference case was calculated for the "Concavity" case, for an error magnitude of 20 μm (increase of 11 °C for normal load and 10 °C for double load). The maximum temperature for the "Convexity" and "One-wave waviness" cases changes only slightly, (by approximately 2 °C). For the cases of "Three-wave

waviness” and “Five-wave waviness”, when normal load is applied to the bearing, a small (and approximately linear) increase in T_{max} is observed along as the magnitude of the error increases (reaching a maximum of approximately 2 °C). For double load of the bearing, the temperature increase is more pronounced, reaching a maximum of 6.5 °C, whereas the changes in maximum temperature, up to an error magnitude of 15 μm, are similar to those corresponding to the “Concavity” case.

The friction power losses of the studied thrust bearing change only slightly for different types and magnitude of manufacturing errors (Fig. 8 d). From basic principles, shear losses depend on (a) the velocity gradient across the film thickness, and (b) the viscosity of the oil, which decreases with increasing temperature. Based on the numerical results, it can be concluded that with the increase of the error magnitude, the oil shear losses remain almost unchanged (maximum variance ± 1.5%) or increase slightly (by max. 5%) depending on the shape of surface error and bearing load. An interesting case is the pad with a concavity surface error. In this particular case, for normal bearing load (680 kN), the largest increase in shear loss in the film, in comparison to that of the reference case, is observed (for a 20 μm error magnitude, power losses increase by about 5 kW, i.e. ~ 5%). On the other hand, for the double bearing load (1360 kN), power losses for this type of surface error are the smallest (less than 0.5 kW decrease in comparison to the reference case). This is due to the favorable change in the proportion of components influencing the oil shear resistance (changes in h_{min} and T_{max}), due to reduction in the film after increasing the load, compared to other cases of sliding surface geometry errors.

In Fig. 9, the calculated pressure, film thickness and sliding surface temperature profiles for two selected shape errors, i. e., for the “One-wave waviness” and “*Concavity*” errors, are presented. The selected shape errors, as confirmed by the results of Fig. 8, demonstrated pronounced changes in the calculated bearing parameters as a function of the increasing error magnitude. Therefore, it is interesting to study and compare the changes in the profiles of the bearing parameters listed, as a function of the error magnitude. In particular, comparison of pressure profiles (Fig. 9 a) indicates contradicting trends of changes as a function of the increasing magnitude of the shape error for the analyzed cases. For the “*One-wave waviness*” error, as the height of the wave increases, the pressure in the central part of the segment increases, while it decreases at the inflow and outflow zones. For the “*Concavity*” case, the trend is reversed, while the differences between pressure values in comparison to the reference case are hardly noticeable. The pressure distribution in the film is closely related to the geometry of the oil gap (Fig. 9 b). The shape of the lubrication gap in the circumferential direction in the case of a waviness error, together with the increasing wave amplitude, can be divided into two areas: inlet with the bottom of the wave (playing a role similar to the lubricating pocket) and outlet with the wave ridge (performing a role similar to the hydrodynamic dam). In the inlet zone of such a gap, the film is thicker (causing lower pressure in the film). However, in the outlet zone, initially as a result of a significant reduction in the thickness of the film, pressure increases and then in a divergent part of the gap near the outlet edge it drops.

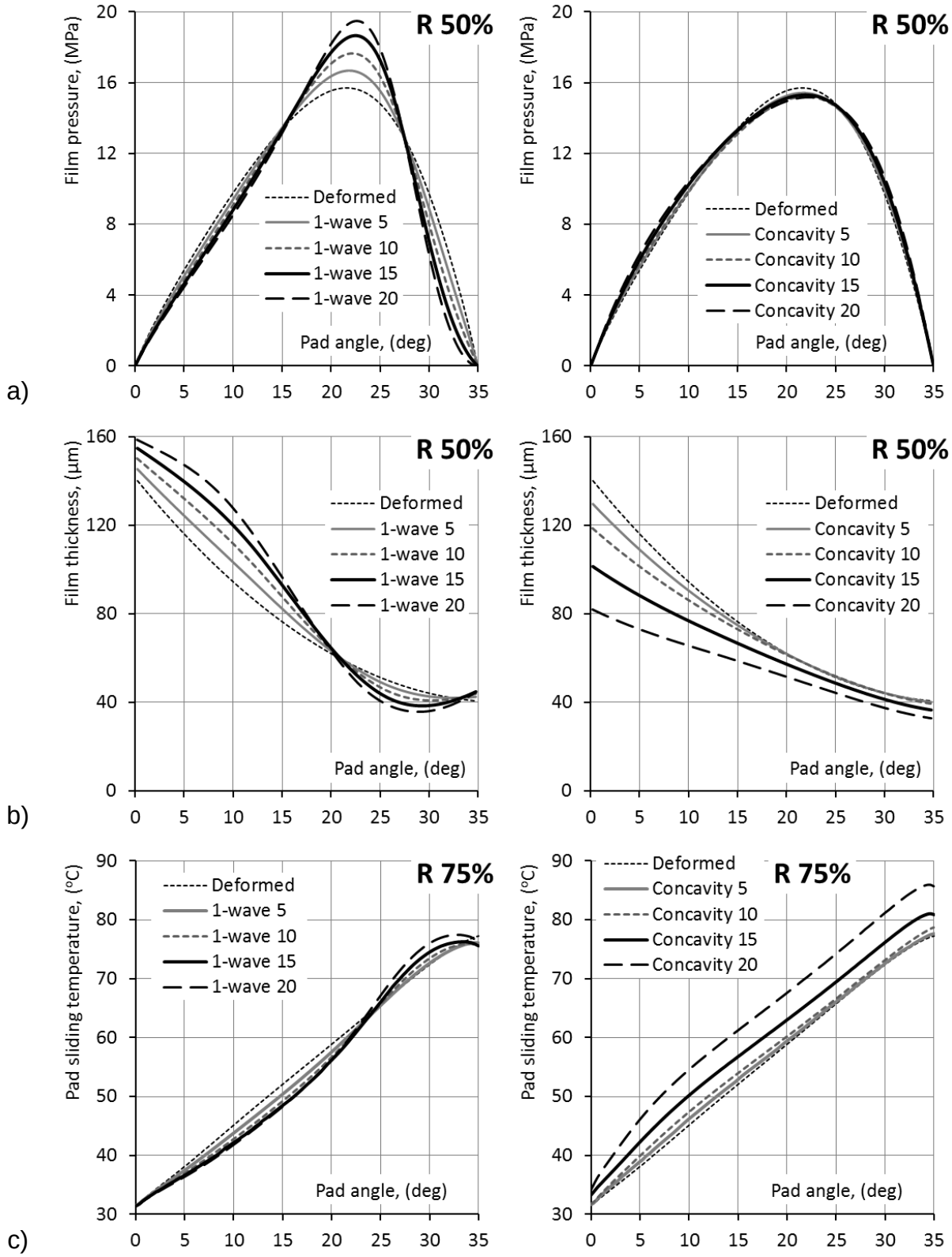

Fig. 9. Comparison of circumferential profiles for the cases of "One-wave waviness" and "Concavity" manufacturing errors with different error amplitudes (double load 1360 kN); a) film pressure at R=50%, b) film thickness at R=50%; c) pad sliding temperature at R=75%.

The pressure distribution and film geometry are in a different way affected by the increasing amplitude of the concavity surface error. It compensates the initial convexity of the segment (resulting from thermo-elastic deformation), as a result of which, the sliding surface becomes less convex and the pressure distribution and shape of the oil

gap becomes similar to the undeformed pad (relatively small circumferential inclination).

The calculated temperature profiles (Fig. 9 c) are also related to the shape of the lubrication gap, and thus also depend on the shape and magnitude of the surface error. Regarding the waviness error, in the zone of thicker film at the inlet, the sliding surface temperature decreases as the magnitude of error amplitude increases. However, in the outlet zone, where the minimum film thickness decreases with the increase of the wave height, the sliding temperature increases as compared to the reference case without shape error. The differences, however, are not significant, being in the range of a few degrees Celsius. Significantly greater differences in temperature values can be observed for the "*Convexity*" case. Together with the increasing error magnitude (compensating for the initial convexity of the thermo-elastic pad deformations), the temperature of the sliding surface along the entire circumferential length increases compared to the case of the reference case. The maximum difference is ~ 10°C for an amplitude of 20 μm. It is also worth noting that the calculated temperatures do not differ much when the shape error magnitude is below 10 μm.

6. Conclusions

The aim of the numerical study of the present paper was the investigation of the effect of sliding surface shape errors on the performance parameters of a large hydrodynamic tilting pad thrust bearing. In general, based on the obtained results, it can be stated that the assumption of non-planar sliding surface of the bearing pad influences substantially the calculated parameters of bearing operation. Depending on the shape of the error, this impact may be beneficial or unfavorable, from the points of view of safety and performance of the bearing.

The main conclusions of the present work are summarized below:

a. As far as the minimum film thickness and the maximum temperature of the sliding surface of the pad are concerned, the concavity of the sliding surface is the least favorable among the analyzed shapes.

b. As far as the maximum film pressure is concerned, the least favorable of the analyzed shapes is the waviness error with a single sine wave.

c. For normal bearing loads, increasing manufacturing error amplitude affects mostly the values of minimum film thickness, whereas at higher bearing loads, the most affected bearing parameter is the maximum film pressure.

d. Friction power losses are comparable for all analyzed cases, and are shown to be only mildly affected by manufacturing errors.

It is noted that surface shape errors may have different character for individual segments of the same bearing, which may cause more pronounced differences in the observed parameters of bearing operation, in comparison to those determined in the present paper.

The obtained results confirm that manufacturing errors of the sliding surface may alter significantly bearing behavior in large tilting pad thrust bearings. The differences observed between experimental and numerical results by many authors (e.g. in [27]), where, despite the use of advanced computational models, significant deviations were found between the calculated and measured bearing operational parameters, may be partially attributed to the lack of considering manufacturing errors in the simulation models. Thus, the present results demonstrate that detailed numerical simulations, including modeling of possible surface manufacturing errors, are imperative in the design stage, for predicting accurately bearing performance and avoiding poor bearing operation in terms of either safety or performance especially for bearings operating under high loads. The analysis should be conducted not only for the anticipated nominal bearing load, but also for additional operating conditions, since the effects of manufacturing errors may lead to more pronounced effects on bearing performance at different bearing loads.

7. References

[1] Burton RA. Effects of two-dimensional, sinusoidal roughness on the load support characteristics of a lubricant film. J Basic Eng 1963;85:258–62. doi:10.1115/1.3656572.

[2] Li J, Chen H. Evaluation on Applicability of Reynolds Equation for Squared Transverse Roughness Compared to CFD. J Tribol 2007;129:963. doi:10.1115/1.2768619.

[3] Pande SS, Somasundaram S. Effect of manufacturing errors on the performance of aerostatic journal bearings. Wear 1981;66:145–56. doi:10.1016/0043-1648(81)90110-1.

[4] Wilson DS. The Effect of Geometry Variations on Hydrodynamic Bearing Performance. A S L E Trans 1966;9:411–9. doi:10.1080/05698196608972157.

[5] Wang X, Xu Q, Wang B, Zhang L, Yang H, Peng Z. Effect of surface waviness on the static performance of aerostatic journal bearings. Tribol Int 2016;103:394–405. doi:10.1016/j.triboint.2016.07.026.

[6] Wang X, Xu Q, Huang M, Zhang L, Peng Z. Effects of journal rotation and surface waviness on the dynamic performance of aerostatic journal bearings. Tribol Int 2017;112:1–9. doi:10.1016/j.triboint.2017.03.027.

[7] Cui H, Wang Y, Yang H, Zhou L, Li H, Wang W, et al. Numerical analysis and experimental research on the angular stiffness of aerostatic bearings. Tribol Int 2018;120:166–78. doi:10.1016/j.triboint.2017.12.040.

[8] Cui H, Wang Y, Yue X, Huang M, Wang W. Effects of manufacturing errors on the static characteristics of aerostatic journal bearings with porous restrictor. Tribol Int 2017;115:246–60. doi:10.1016/j.triboint.2017.05.008.

[9] Cui H, Wang Y, Yue X, Huang M, Wang W, Jiang Z. Numerical analysis and experimental investigation into the effects of manufacturing errors on the running accuracy of the aerostatic porous spindle. Tribol Int 2018;118:20–36. doi:10.1016/j.triboint.2017.09.020.

[10] Shelly P, Ettles C. Effect of Transverse and Longitudinal Surface Waviness on the Operation of Journal Bearings. J Mech Eng Sci 1972;14:168–72. doi:10.1243/JMES_JOUR_1972_014_024_02.

[11] Berthe D, Fantino B, Frene J, Godet M. Influence of Shape Defects and Surface

Roughness on the Hydrodynamics of Lubricated Systems. J Mech Eng Sci 1974;16:156–9. doi:10.1243/JMES_JOUR_1974_016_029_02.

[12] Frene J, Nicolas D, Degueurce B, Berthe D, Godet M. Hydrodynamic Lubrication - Bearings and Thrust Bearings (Tribology Series, 33). Elsevier; 1997.

[13] Cui S, Gu L, Fillon M, Wang L, Zhang C. The effects of surface roughness on the transient characteristics of hydrodynamic cylindrical bearings during startup. Tribol Int 2018;128:421–8. doi:10.1016/j.triboint.2018.06.010.

[14] Fillon M, Bouyer J. Thermohydrodynamic analysis of a worn plain journal bearing. Tribol. Int., vol. 37, 2004, p. 129–36. doi:10.1016/S0301-679X(03)00051-3.

[15] Litwin W. Influence of local bush wear on water lubricated sliding bearing load carrying capacity. Tribol Int 2016;103:352–8. doi:10.1016/j.triboint.2016.06.044.

[16] Dobrica MB, Fillon M. Performance degradation in scratched journal bearings. Tribol Int 2012;51:1–10. doi:10.1016/j.triboint.2012.02.003.

[17] Charitopoulos AG, Efstathiou EE, Papadopoulos CI, Nikolakopoulos PG, Kaiktsis L. Effects of manufacturing errors on tribological characteristics of 3-D textured micro- thrust bearings. CIRP J Manuf Sci Technol 2013;6:128–42. doi:10.1016/j.cirpj.2012.12.001.

[18] Papadopoulos CI, Kaiktsis L, Fillon M. Computational Fluid Dynamics Thermohydrodynamic Analysis of Three-Dimensional Sector-Pad Thrust Bearings With Rectangular Dimples. J Tribol 2013;136:011702. doi:10.1115/1.4025245.

[19] Fouflias DG, Charitopoulos AG, Papadopoulos CI, Kaiktsis L, Fillon M. Performance comparison between textured, pocket, and tapered-land sector-pad thrust bearings using computational fluid dynamics thermohydrodynamic analysis. Proc Inst Mech Eng Part J J Eng Tribol 2015;229:376–97. doi:10.1177/1350650114550346.

[20] Fillon M, Wodtke M, Wasilczuk M. Effect of presence of lifting pocket on the THD performance of a large tilting-pad thrust bearing. Friction 2015;3. doi:10.1007/s40544-015-0092-4.

[21] De Pellegrin D V., Hargreaves DJ. An isoviscous, isothermal model investigating the influence of hydrostatic recesses on a spring-supported tilting pad thrust bearing. Tribol Int 2012;51:25–35. doi:10.1016/j.triboint.2012.02.008.

[22] Li S, An Q. Lubrication performance of planar thrust bearing with consideration of roughness of the surfaces. Proc Inst Mech Eng Part J J Eng Tribol 2018:135065011881381. doi:10.1177/1350650118813818.

[23] Roylance BJ. Radially Grooved Thin Plate Thrust Washers: Factors Affecting Their Performance. J Lubr Technol 1975;97:565–9.

[24] Charitopoulos A, Fillon M, Papadopoulos CI. Numerical investigation of parallel and quasi-parallel slider bearings operating under ThermoElastoHydroDynamic (TEHD) regime. Tribol Int 2018. doi:10.1016/j.triboint.2018.12.017.

[25] Dąbrowski L, Wasilczuk M. Evaluation of water turbine hydrodynamic thrust bearing performance on the basis of thermoelastohydrodynamic calculations and operational data. Proc Inst Mech Eng Part J J Eng Tribol 2004;218:413–21. doi:10.1243/1350650042128094.

[26] Wodtke M, Fillon M, Schubert A, Wasilczuk M. Study of the influence of heat convection coefficient on predicted performance of a large tilting-pad thrust bearing. J Tribol 2013;135. doi:10.1115/1.4023086.

[27] Wodtke M, Schubert A, Fillon M, Wasilczuk M, Pajaczkowski P. Large hydrodynamic thrust bearing: Comparison of the calculations and measurements. Proc Inst Mech Eng Part J J Eng Tribol 2014;228. doi:10.1177/1350650114528317.